PPPL-2357

MEASUREMENTS OF THE TOROIDAL PLASMA ROTATION VELOCITY IN TFTR MAJOR-RADIUS COMPRESSION EXPERIMENTS WITH AUXILIARY NEUTRAL BEAM HEATING

By

M. Bitter et al.

JULY 1986

PLASMA PHYSICS LABORATORY

PRINCETON UNIVERSITY
PRINCETON, NEW JERSEY

PREPARED FOR THE U.S. DEPARTMENT OF ENERGY,
UNDER CONTRACT DE-AC02-76-CHO-3073.

NOTICE

Printed in the United States of America

Available from:

National Technical Information Service
U.S. Department of Commerce
5285 Port Royal Road
Springfield, Virginia 22161

Price Printed Copy $ * ; Microfiche $4.50

*Pages	NTIS Selling Price
1-25	$7.00
25-50	$8.50
51-75	$10.00
76-100	$11.50
101-125	$13.00
126-150	$14.50
151-175	$16.00
176-200	$17.50
201-225	$19.00
226-250	$20.50
251-275	$22.00
276-300	$23.50
301-325	$25.00
326-350	$26.50
351-375	$28.00
376-400	$29.50
401-425	$31.00
426-450	$32.50
451-475	$34.00
476-500	$35.50
500-525	$37.00
526-550	$38.50
551-575	$40.00
567-600	$41.30

For documents over 600 pages, add $1.50 for each additional 25-page increment.

MEASUREMENTS OF THE TOROIDAL PLASMA ROTATION VELOCITY IN TFTR MAJOR-RADIUS COMPRESSION EXPERIMENTS WITH AUXILIARY NEUTRAL BEAM HEATING

M. Bitter, S. Scott, K. L. Wong, R. J. Goldston, B. Grek, S. von Goeler, R. J. Hawryluk, K. W. Hill, H. Hsuan, D. Johnson, S. Sesnic, G. Tait, and M. C. Zarnstorff

PPPL--2357

DE86 013641

Princeton University, Plasma Physics Laboratory

Princeton, NJ 08544

Abstract

The time history of the central toroidal plasma rotation velocity in Tokamak Fusion Test Reactor (TFTR) experiments with auxiliary heating by neutral deuterium beam injection and major-radius compression has been measured from the Doppler shift of the emitted TiXXI-Kα line radiation. The experiments were conducted for neutral beam powers in the range from 2.1 to 3.8 MW and line-averaged densities in the range from 1.8 to 3.0 × 10^{19} m^{-2}. The observed rotation velocity increase during compression is in agreement with results from modeling calculations which assume classical slowing-down of the injected fast deuterium ions and momentum damping at the rate established in the precompression plasma.

I. Introduction

In a previous paper [1] we presented results from major-radius compression experiments in the Tokamak Fusion Test Reactor (TFTR). These experiments showed an acceleration of tangentially injected deuterium beam ions from 82 to 150 keV, a variation of the energy spectra of charge-exchanged neutrals and a substantial increase of the neutron and proton yield from $d(d,n)^3He$ and $^3He(d,p)\alpha$ reactions. Also observed was a sudden increase of the beam-induced toroidal rotation of the bulk plasma during compression. The toroidal rotation of tokamak plasmas with intense neutral beam injection has been a subject of research in recent years [2-5]. Investigation of the toroidal plasma rotation in major-radius compression experiments is of particular interest since these experiments provide information on the angular momentum conservation of the bulk plasma, in a case where the plasma is detached from material limiters and the energy associated with plasma rotation is not provided solely by neutral beam injection. In our experiments the deuterium beam injection was turned off immediately before compression, but after the toroidal rotation velocity had reached an equilibrium value. Thus, if one assumes no net angular momentum input during the compression, one would expect v_ϕ to increase by a factor $C = R(t = 0)/R(t = \infty)$ corresponding to the compression ratio, provided that the velocity profile remains unchanged. In our experiments the observed increase in v_ϕ was typically smaller due to the fact that viscous damping during the compression could not be neglected.

In this paper we present experimental results on the toroidal rotation velocity in TFTR major-radius compression experiments for a range of plasma densities, plasma currents, and neutral beam powers, and compare the data with modelling calculations. It is found that the observed velocity increase during compression is consistent with classical slowing-down of the injected

deuterium ions and viscous angular momentum damping at the rate established in the precompression plasma.

The experimental results are presented in Sec. II. The modelling calculations are described in Sec. III.

II. Experimental Results

The toroidal plasma rotation velocity has been obtained from measurements of the Doppler shift of the Ti XXI Kα resonance line at $\lambda = 2.6097$Å by a Bragg bent crystal spectrometer of high spectral resolution ($\lambda/\Delta\lambda = 25000$ at $\lambda = 2.61$Å). Since the Ti XXI ions are produced in the hot core of the plasma and since the 1s-2p resonance transition is collisionally excited by electrons with energies in excess of 4.75 keV, the Ti XXI radiation can be used for the diagnosis of the central plasma parameters. A description of the spectrometer and a detailed comparison of the observed Ti XXI spectra with atomic theories have been given in Refs. 6 and 7.

A schematic of the experimental arrangement is shown in Fig. 1, representing a quadrant of the TFTR vacuum vessel, the pre(post)compression plasmas with major and minor radii of R = 3.00 m, a = 0.57 m (R = 2.17 m , a = 0.48 m), respectively, and the line of sight of the spectrometer. The precompressed deuterium plasma was heated by neutral deuterium beam injection during the time interval from 2.3 to 2.5 sec. Adiabatic compression of the plasma started upon termination of the neutral beam injection and was completed by 2.520 sec. Figure 2 presents the time history of the plasma displacement in major radius, R(t), during the compression, as determined from the position of the peak density obtained by Thomson scattering measurements from several discharges with nearly identical parameters. The curve shown in Fig. 2 represents a least mean squares fit to the data points. This curve is

used as a representation of R(t) for the analysis of our experimental results. The plasma displacement during compression has also been determined from density profile measurements of a multichannel infrared interferometer (MIRI) and from magnetic field measurements. The results obtained from the different diagnostic techniques were in good agreement.

The Doppler shift, $\Delta\lambda$, observed by the spectrometer is given by the expression (1):

$$\Delta\lambda = \frac{\lambda}{c} v_\phi \sin\alpha \quad , \tag{1}$$

where λ = 2.6097Å is the wavelength of the Ti XXI Kα line, c the velocity of light, and v_ϕ the toroidal rotation velocity of the Ti XXI ions. Calculations of classical collisional coupling between the impurity and bulk ions indicate that v_ϕ also represents the toroidal velocity of the bulk plasma. α is the angle of the intersection between the spectrometer sightline and the radial direction at the center of the plasma as indicated in Fig. 1. Thus

$$R_o \cdot \sin\alpha = D = \text{constant} \quad , \tag{2}$$

where R is the major radius at the center of the plasma and D the distance of the spectrometer sightline from a parallel diameter of the torus. Combining Eq. (1) and Eq. (2) we see that the toroidal velocity component seen by the spectrometer is proportional to 1/R, and that the time history of the observed Doppler shift during the compression can be described by expression (3):

$$\frac{\Delta\lambda(t)}{\Delta\lambda(0)} = \frac{v_\phi(t)}{v_\phi(0)} \cdot \frac{R_o(0)}{R_o(t)} \quad , \tag{3}$$

where $R_o0) = 3.00$ m is the major radius of the precompressed plasma and $v_\phi(0)$ the toroidal velocity of the precompressed plasma at the termination of the neutral beam injection. With the assumption of angular momentum conservation, $R_o \cdot v_\phi$ = constant, we obtain:

$$\frac{\Delta\lambda(t)}{\Delta\lambda(0)} = \left(\frac{R_o(0)}{R_o(t)}\right)^2 \quad . \tag{4}$$

Equation (4) cannot be applied directly to our data because of two effects: (1) The compression time is not short relative to the momentum confinement time. (2) Momentum continues to be deposited to the bulk plasma during the compression by fast beam ions. These effects will be considered in detail in Sec. III. In this section we interpret the data using Eq. (4) to obtain bounds on these effects.

Compression experiments were performed for several different discharge parameters: The plasma current, I_p, was 450 kA before compression and 622 kA after compression. The line-integrated density, $\int n_e d\ell$, before compression was in the range from 1.8 to 3.0 $\times$ 10^{19} m^{-2} and the injected neutral beam power, P_b, was in the range from 2.1 to 3.8 MW. In these experiments, intense emission of the Ti XXI Kα line was observed with typical count rates of 2 $\times$ 10^5 photons/sec. The high count rate allowed us to record Ti XXI Kα line spectra with a time resolution of 10 msec and to perform Doppler shift measurements with a small statistical error. Since the spectrometer electronics is able to record 128 separate spectra during a TFTR discharge of typically four seconds, we have chosen time bins of different lengths, i.e., time bins of 10 msec for the period from 2.300 to 3.260 sec and time bins of 80 msec outside this time interval, in order to monitor the Ti XXI Kα line radiation during the whole discharge. Since the spectrometer has no absolute

wavelength calibration, the wavelength shift of the Ti XXI Kα line has been measured with reference to its center position during the steady-state part of the ohmic heating phase at 2.250 sec, before the neutral beam injection. This reference value was reproducible to within 2×10^{-5} Å due to the fact that the central electron temperature during the steady-state part of the ohmic heating phase was above 2 keV, so that wavelength shifts of the apparent Ti XXI Kα line due to the presence of unresolved dielectronic satellites were negligible. Dielectronic redshifts of the order of 1×10^{-4}Å, which can occur at electron temperatures below 2 keV, have been observed at the beginning of the discharge when the central electron temperature was still rising and they have been discussed quantitatively in Ref. 7.

Figure 3 presents a time history of the observed Doppler shifts of the Ti XXI Kα resonance line. The data were obtained from discharges with $\int n_e d\ell = 1.8 \times 10^{19}$ m^{-2} and $P_b = 2.1$ MW. Figures 3a, b show the results from a single discharge and, respectively, the results from the accumulated data of eight discharges with nearly identical parameters. The statistical error of the data is indicated by the vertical error bars in Fig. 3a. The horizontal bars indicate the lengths of the time bins used for the data collection or the time average of the raw spectral data. For the 10 ms time bins the horizontal bars are of the size of the data points. The accumulation of raw data from different discharges allows us to further reduce the statistical error and to average out time variations of the line center position due to sawtooth events in individual discharges. The occurrence of a sawtooth event during the time from 2.450 to 2.480 sec is clearly seen in the data shown in Fig. 3a. The statistical error bar of the accumulated data shown in Fig. 3b is of the size of the data points.

We infer from Fig. 3b that, with the beginning of the neutral deuterium

injection at 2.3 sec, the center position of the Ti XXI Kα line is shifted from its value during the ohmic heating phase, which is represented by the data point 1, and that it reaches a new equilibrium value after 120 msec, well before termination of the injection at 2.5 sec. This equilibrium value $v_\phi(0)$ is found to scale in an offset linear fashion with the ratio of beam power and plasma density as shown in Fig. 4. Since we use as a reference for our Doppler shift measurements the center position of the Ti XXI Kα line during the steady-state part of the ohmic heating phase, we obtain, by definition, $v_\phi(0) = 0$ for $P_b = 0$. The v_ϕ-intercept of 5×10^4 m sec^{-1} obtained by the linear extrapolation of the data points for $P_b > 0$ in Fig. 4, therefore, indicates that the momentum confinement deteriorates with increasing neutral beam power. [A similar offset linear scaling with a v_ϕ-intercept of 4×10^4 m sec^{-1} and a slope of $\Delta v_\phi / \Delta(P_b/\bar{n}_e) = 1.18 \times 10^{18}$[W^{-1} m^{-2} sec^{-1}] (which is by a factor 1.75 larger than the slope of the straight line shown in Fig. 4) has been observed in neutral beam heating experiments of large (R = 2.55 m, a = 0,81 m) TFTR plasmas [8]]. A further increase of the wavelength shift is clearly seen during the compression phase, which extends from 2.500 to 2.520 sec. Unfortunately, our measurements are impaired at the time of 2.530 sec by the onset of mechanical vibrations of the TFTR vacuum vessel at a frequency of 35 Hz. This frequency is the characteristic frequency of a mechanical oscillation mode of the TFTR vacuum vessel, which is excited during the compression phase. Although the spectrometer was not in direct contact with the TFTR vacuum vessel, mechanical oscillations can be coupled to the spectrometer by sound propagation through the air and the concrete floor of the TFTR test cell. The estimated time for sound propagation from the vacuum vessel to the crystal is ~15 msec. Since the distance between the crystal and the X-ray detector is 3.5 m, mechanical vibrations of the crystal with

amplitudes of a few microns are sufficient to explain the observed effects. The observed oscillation pattern of the Ti XXI Kα line center position is very reproducible both in phase and amplitude. This is evident from the data points in Figs. 3a and 3b, which represent the data from a single discharge and the accumulated data from eight discharges, respectively. The onset of a 35 Hz oscillation at the end of the compression phase has also been observed by other diagnostics, e.g., by the interferometers used for density measurements. Since the time resolution of these diagnostics is better than 1 msec, we are confident that the frequency inferred from the dashed line in Fig. 3b is correct.

Our analysis of the time history of the toroidal rotation velocity during the compression experiment is based on the data points 1, 2, 3, 4, and 5 in Fig. 3b. The data points 1 and 2 were used to determine the toroidal velocity of the precompressed plasma at the end of the neutral beam injection, whereas the data points 3, 4, and 5 were used to derive the increase of the rotation velocity during the compression phase. The data represented by point 5 are presumably affected by mechanical oscillations and are thus not very certain. The estimated uncertainty in point 4 due to the oscillations is comparable to the observed scatter in the data shown in Fig. 5. We have included these data in the analysis, since the oscillation amplitude is still small at the onset. The data collected at times $t > 2.530$ sec are strongly affected by the mechanical oscillations and must be evaluated with caution. In order to interpret these data, we have assumed that the plasma reaches a new equilibrium state after the compression and that the equilibrium position of the Ti XXI Kα line can be found by averaging the data over time intervals which are large compared with the period of the mechanical oscillations. Figure 3c presents the results obtained by averaging the raw data of the post-

compression plasma shown in Fig. 3b over time intervals of 40 msec. These time-averaged data indicate an exponential decay of the toroidal rotation velocity with a time constant of 310 msec represented by the dashed curve in Fig. 3c. The exponential has been determined from a least mean squares fit to the eight data points shown in Fig. 3c in the time interval from 2.610 to 3.250 sec. The datum point in the time interval from 2.530 to 2.610 sec has not been included for determination of the fit, since we assumed that the plasma still contained a substantial amount of fast beam particles. The value of 310 msec for the decay time of v_ϕ is comparable with the values obtained for TFTR noncompression experiments with neutral beam injection for R = 2.55 m and a = 0.81 m. In these experiments, the Doppler shift measurements were not impaired by interferences from mechanical oscillations.

Before we discuss our modeling calculations we compare the experimental results with the predictions of Eq. (4). Equation (4) is applicable in the asymptotic limit that viscous damping and torque deposition during the compression phase can be neglected. By comparing the experimental data with the predictions from Eq. (4), we obtain upper bounds on the sum of these effects. Figure 5 represents the observed time history of the wavelength shift during the compression phase for the investigated range of neutral beam powers and plasma densities. The experimental points represent accumulated raw data from nearly identical discharges for the data of the five selected time bins shown in Fig. 3b. The wavelength shifts have been normalized to the value, $\Delta\lambda(0)$, observed in the precompressed plasma at the end of the neutral beam injection. This value was derived from the data in the time bins 1 and 2. The predictions of Eq. (4) are shown by curve (a). The values of $[R_o(0)/R_o(t)]^2$ have been calculated from the curve fit to the experimental data shown in Fig. 2. The staircase curve (b) represents time-averaged values

of $[R_o(o)/R_o(t)]^2$ for successive time intervals of 10 msec corresponding to the time resolution of the $v_\phi(t)$ measurements. This curve should be compared with the experimental data. The time-averaged values represented by curve (b) are not very sensitive to the shape of R(t) and are consequently not strongly affected by experimental uncertainties in the determination of R(t) from the Thomson scattering data. Curve (c) shows the shift that would be observed if the major plasma radius changed with time according to the curve in Fig. 2, but v_ϕ remained constant. It is evident from Fig. 4 that the experimental data points are well above this curve. This clearly indicates that the toroidal velocity, v_ϕ, increases during the compression. The experimental points are, however, below the values of the curve (b) predicted by Eq. (4) indicating the importance of the neglected effects of the finite momentum confinement time.

III. MODELING CALCULATIONS

The time history of rotation velocity was calculated numerically by a 1-D momentum transport simulation to elucidate the combined effects of viscous damping and torque deposition during the compression stroke. These calculations were performed to determine whether the velocity increase measured during compression (28%) is consistent with classical beam ion slowing down and angular momentum conservation under conditions where the compression time (≈ 15 ms) is not significantly shorter than the precompression momentum confinement time (≈ 35 ms). The velocity simulation model incorporates a number of free parameters, such as the magnitude of the momentum diffusivity, whose values were adjusted to best reproduce the time history of central rotation speed prior to compression. However, these values were held fixed during the compression stroke, so that by comparing the

calculated velocity increase during compression with the measured increase, we can determine whether the momentum confinement time changes during compression.

Under the assumptions of circular, concentric flux surfaces, excluding the explicit term for convective momentum transport, and simplifying to a mean-ion species model, Goldston's formulation of the momentum balance [9] can be written:

$$mn\left[\frac{\partial}{\partial t}\left(Rv_\phi\right)\right]_{r/a} + \frac{mv_\phi}{a^2}\left[\frac{\partial}{\partial t}\left(nRa^2\right)\right]_{r/a} = r_a(r,t) + \frac{1}{r}\frac{\partial}{\partial r}\left(r\bar{R}nm\chi_\phi\frac{\partial v_\phi}{\partial r}\right) - \frac{nmRv_\phi}{\tau_{\phi cx}} \quad , \tag{5}$$

where n is the ion density, m is the mean ion mass, $\tau_{\phi cx}$ is the charge-exchange time for toroidal momentum loss, and χ_ϕ is the momentum diffusivity. Here $r_a(r,t)$ is the total torque density delivered to the plasma from the beams, including a collisional contribution which is delivered over roughly a fast-ion slowing down time, and a "prompt" contribution which is delivered nearly instantaneously, over the fast ion's first poloidal orbit. All damping including convective momentum losses, but excluding charge-exchange losses is incorporated into the perpendicular viscosity, χ_ϕ. A separation of the total radial transport of momentum into viscous and convective components as discussed by Goldston [9] is not important for the present modeling calculations, since our primary interest is the central velocity increase during compression.

The time derivatives in Eq. (5) are evaluated on a surface of constant r/a. The second term on the left-hand side of Eq. (5) represents the time derivative of stored angular momentum due to changes in the number of ions in the plasma. It is an important term in the angular momentum balance during

beam injection because beam fueling significantly increases the plasma density. (Density increases of $\Delta n_e/n_e$ ~ 40% - 100% are typical in these experiments.) During and following compression, this term is small because the plasma density decays slowly.

To calculate the collisional contribution of the torque delivered to the plasma as a function of time and radius, each of the three neutral beam sources was represented by a set of eight pencil beamlets, spaced vertically, whose relative weights were consistent with a Gaussian beam profile of width 18 cm [i.e., $P(z) = P_0 \exp[-(z/18)^2]$. The current of each pencil beamlet for each beam energy component was estimated from the total beam source power, beam source energy, and the beam energy component mix. (The ratios of the atomic currents at the full, half, and third energies are $I_1:I_{1/2}:I_{1/3}$ = 27:33:40.) The time history of beam torque in each shell deposited by collisional damping was obtained by calculating analytically the time required for the beam ions to lose their initial $v_\parallel$ due to pitch-angle scattering and slowing down. The model neglects the influence of the target plasma's rotation speed on the cross sections for beam neutral ionization, as well as beam ion losses due to charge exchange and unconfined orbits, since these terms were shown to be small using a time-independent Fokker-Planck torque deposition code at a single time point just prior to compression. The largest error was found to be the neglect of lost deposited torque (10%) due to beam ion charge exchange.

To estimate roughly the magnitude of the prompt torque deposition, we note that a near parallel fast ion which is born at the horizontal midplane on the large-major-radius side of a flux surface ($R = R_0 + r$) with some angular momentum $m \cdot R \cdot v_{\parallel 0}$ obtains, on its first few poloidal orbits, a time-averaged angular momentum of approximately $m \cdot R \cdot v_{\parallel 0}(1-\epsilon)$, where $\epsilon = r/a$.

Thus, a factor ~ε of the torque is deposited promptly, and this factor was incorporated into the numerical torque deposition model. Including the prompt torque term allowed the rotation simulation to better reproduce the measured v_ϕ during the first 100 ms of neutral injection, but its effect on the calculated velocity rise during compression was small.

The charge-exchange term of Eq. (5) was negligible at the plasma center, and became significant only near the plasma edge. The characteristic time for charge-exchange loss of angular momentum is $\tau_{\phi cx} = \tau_{cx} \times v_\phi(r)/[v_\phi(r)-v_{\phi o}(r)]$, where $v_{\phi o}(r)$ is the velocity of the neutral prior to charge exchange, and $\tau_{cx} = 1/n\langle\sigma v\rangle_{cx}$. The neutral density was calculated by a standard 1-D neutrals code (FRANTIC) [10,11] including the beam halo contribution. As suggested by Suckewer et al., [3] we approximated the quantity $[v_\phi(r)]/[v_\phi(r)-v_{\phi o}(r)]$ by the quantity $h = T_i(r)/[T_i(r) - T_{io}(r)]$, where $T_{io}(r)$ is the calculated neutral temperature. Under these assumptions, less than 10% of the total input torque was dissipated by charge exchange.

Two features of Eq. (5) deserve additional comment. First, neglecting convective losses of ions during compression ("classical" compression scaling of density), then nRa^2 = constant, so the second term of the left-hand side of Eq. (5) would be zero. In the asymptotic limit discussed in section I, which assumes classical compression scaling of the density and which neglects both viscous damping and torque deposition during compression, the right-hand side of Eq. (5) is zero, so we recover the classical result, $v_\phi \propto C$ $R_o(t = 0)/R_o(t = \infty) = 1.38$. The second interesting feature of Eq. (5) is that, since the plasma rotation speed has reached a quasi-equilibrium state prior to compression, the right-hand side of Eq. (5) is also nearly zero just prior to compression because the torque deposition is balanced by viscous damping. This cancellation of terms explains the somewhat paradoxical result

of the full velocity simulation which predicts a velocity increase of 28% — surprisingly close to the asymptotic limit of 38%, considering that the viscous damping considered alone (i.e., neglecting torque deposition following beam turnoff) would have resulted in a velocity decrease by a factor of $C \times \exp(-15\ \text{ms}/35\ \text{ms}) = 0.90$. In the full velocity simulation, the calculated velocity increase during compression falls short of the asymptotic limit because the instantaneous torque during compression is less than the precompression value (owing to the loss of prompt torque component and the longer slowing down time), whereas the χ_ϕ is assumed constant.

The velocity simulation requires that we specify the momentum diffusivity as a function of radius and time. Lacking profile measurements of $v_\phi(r)$, one has considerable latitude to define the radial dependence of χ_ϕ. We find that the time history of the rotation speed prior to compression is reproduced quite well using a momentum diffusivity of the form

$$\chi_\phi(r,t) = 0.63\ \left[1 + 3\left(\frac{r}{a}\right)^2\right]\left(1 + 0.133 \times \Gamma_a\right)\ \frac{m^2}{s} \qquad (6)$$

with no explicit time dependence (Fig. 6a). The radial profile factor yields a nearly parabolic shape of v_ϕ.

The quantity Γ_a in Eq. (6) represents the total torque delivered to the plasma rather than a local torque density. Effectively it causes the calculated momentum confinement time to decrease with increasing beam power (e.g., χ_ϕ would increase by a factor 1.7 as the beam power is increased from 1.0 → 4.0 MW). The form for χ_ϕ in Eq. (6) is consistent with our observation that at fixed plasma current and plasma density (I_p = 450 kA, $\bar{n}_e = 1.8 \times 10^{19}$ m^{-3}), the central rotation speed rises linearly with applied beam power P_b in the range from 1.0 to 4.0 MW but with an apparent offset of $3 - 5 \times 10^6$ cm/sec

at zero beam power. If χ_ϕ is chosen to be independent of applied torque, but adjusted to match $v_\phi(0)$ at the end of the neutral beam injection, then the velocity simulation underestimates the measured central rotation speed for the first 100 ms of neutral injection, but the calculated increase in $v_\phi(0)$ following compression is changed only slightly. Similarly, our conclusions regarding the compression scaling of rotation speed are insensitive to the assumed radial variation of χ_ϕ.

The momentum diffusivity $\chi_\phi(r,t)$ was represented by the expression in Eq. (6) during both the beam-heated, precompression phase of the discharge and during compression until t = 2.520 sec. To allow the best possible comparison of the expected velocity rise during compression with the experimental data, the magnitude of χ_ϕ was chosen carefully to reproduce the measured v_ϕ just prior to compression at t = 2.500 sec. The results of the velocity simulation are shown in Fig. 6. The velocity simulation predicts an increase $\Delta v_\phi/v_\phi$ of 28% during the compression stroke, in excellent agreement with the measured $v_\phi(t)$. Thus, if we fix the viscous momentum damping at the precompression rate and account for torque deposition during the compression stroke due to classical fast ion slowing down, then the measured rotation increase due to compression is in agreement with angular momentum conservation.

Figure 6c shows the time history of the characteristic time for loss of parallel velocity by the energetic beam ions, τ_s, which determines how quickly the deposited torque decays following termination of beam injection. Here τ_s is averaged over all beam sources and beam energy components, and averaged over the plasma volume. The characteristic deposition time τ_s increases during compression, despite the rising electron density, because the fast ion energy is also pumped by compression.

To simulate accurately $v_\phi(t)$ <u>beyond</u> the end of compression (t > 2.520

sec) in the transport code, it was necessary to reduce substantially $\chi_\phi(t)$. The portion of the simulation for which $\chi_\phi(r,t)$ was artificially reduced is indicated by a dashed line in Fig. 6a. In the simulation $\chi_\phi(r,t)$ was reduced by a factor of 0.65 starting at t = 2.520 sec, decreasing to a factor of 0.1 at t = 2.900 sec. This behavior is best illustrated in Fig. 6b, where we plot the time history of global momentum confinement time, $\tau_\phi(t)$, as calculated from the simulated velocity,

$$\tau_\phi(t) = \frac{\int mnRv_\phi(r,t)\, dV}{\Gamma_a(t) - \frac{\partial}{\partial t}\int mnRv_\phi(r,t)\, dV} \quad . \tag{7}$$

Similar to the behavior of large-core TFTR plasmas, the momentum confinement time as calculated from Eq. (7) increased to several hundred milliseconds after the beam ions slowed down. This calculated momentum confinement time is somewhat shorter than the velocity decay time (≈310 ms) because it includes velocity profile effects, density decay, and the small torque deposition following beam turnoff.

To evaluate the possibility that ripple damping of toroidal momentum could be responsible for the rather short momentum confinement times in the precompression plasmas (τ_p = 35 ms vs 80 ms in the standard TFTR plasma), we calculated the expected damping rates for the ripple plateau (rp) and ripple trapping (rt) transport mechanisms. The TFTR precompression plasmas are formed at large major radius (R = 299 cm). They extend somewhat closer to the toroidal field coils and, consequently, they experience a considerably greater vacuum field ripple than standard TFTR plasmas. The peak-to-average vacuum ripple in the precompression configuration is 1.8% at the plasma edge and 0.08% at the plasma center, compared to an edge ripple of 0.5% in the standard (r/a = 2.55/0.83 m) configuration. The theoretical expressions for the

momentum damping times due to ripple viscosity are [12]:

$$\tau_\phi^{rp} = \rho_{\theta i}^2 / D^{rp} \quad , \tag{8}$$

$$\tau_\phi^{rt} = \rho_{\theta i}^2 / D^{rt} \quad , \tag{9}$$

where $\rho_{\theta i}$ is the ion poloidal gyroradius and D^{rp} and D^{rt} are the nonambipolar ion ripple diffusion coefficients. The calculation of D^{rp} and D^{rt} were flux-surface averaged to account for the strong variation of ripple strength with poloidal angle, using the measured density profile and an ion temperature profile derived from a neoclassical ion power balance (the central T_i was matched to the value measured by Ti-K_α Doppler broadening = 4.0 keV). The expression for D^{rp} is taken from Boozer [13]. The expression for D^{rt} includes a correction for the boundary-layer contribution [14] as well as classical ripple-trapping viscosity [15-17].

Both mechanisms provide negligible momentum damping at the plasma center [$\tau^{rp}(0)$, $\tau^{rt}(0)$ > 300 ms]. Over the region r = 20 - 45 cm, τ^{rp} obtains a broad minimum of 140-180 ms. The ripple trapping damping term reaches a minimum of 160 ms at r = 45 cm. The combined effect of both ripple transport mechanisms yields a theoretical momentum damping time in excess of 80 ms throughout the entire plasma, more than twice the measured value. While this result suggests that ripple is not the mechanism responsible for the short τ_ϕ obtained in the precompression plasmas, we add two cautionary remarks: (1) Controlled ripple experiments on ISX-B [18] found that the theoretical ripple transport underestimated the measured momentum transport due to ripple by a factor ~6; and (2) The theoretical calculations are dependent on some poorly known quantities, such as the radial profile of ion temperature.

ACKNOWLEDGMENTS

We gratefully acknowledge the many engineers, computer programmers, technicians, and other TFTR staff members who contributed to this work, and we also appreciate the continuous support from Dr. H. P. Furth, Dr. D. Grove, Dr. P. Rutherford, Dr. D. Meade, Dr. K. M. Young, and Dr. L. C. Johnson.

This work supported by United States Department of Energy Contract No. DE-AC02-76-CHO-3073.

REFERENCES

[1] K.L. Wong , M. Bitter, G.W. Hammett, W. Heidbrink, H. Hendel, et al., Phy. Rev. Lett. 55 (1985) 2587.

[2] R.C. Isler, L.E. Murray, S. Kasai, D.E. Arnurius, S.C. Bates, et al., Phys. Rev. Lett. 47 (1981) 649.

[3] S. Suckewer, H. P. Eubank, R. J. Goldston, J. McEnerney, N. R. Sauthoff, H. H. Towner, Nucl. Fusion 21 (1981) 1301.

[4] K. Brau, M. Bitter, R.J. Goldston, D. Manos, K. McGuire, and S. Suckewer, Nucl. Fusion 23 (1983) 1643.

[5] D.J. Grove and D.M. Meade, Princeton Plasma Physics Laboratory Report PPPL-2233 (June 1985).

[6] K.W. Hill, M. Bitter, M. Tavernier, M. Diesso, S. von Goeler, G. Johnson, L.C. Johnson, N.R. Sauthoff, N. Sesnic, F. Tenney, and K. M. Young, Rev. Sci. Instrum. 56 (1985) 1165.

[7] M. Bitter, K.W. Hill, M. Zarnstorff, S. von Goeler, R. Hulse, L.C. Johnson, N.R. Sauthoff, S. Sesnic, K.M. Young, M. Tavernier, F. Bely-Dubau, P. Faucher, M. Cornille, and J. Dubau, Phys. Rev. A 32 (1985) 3011.

[8] M. Murakami, et al., Plasma Phys. Controlled Fusion 28, No. IA (1986) 17-27.

[9] R. J. Goldston, "Topics in Confinement Analysis of Tokamaks With Auxiliary Heating," to be published in proceedings of Course and Workshop on Basic Physical Processes of Toroidal Fusion Plasmas, Varenna, Italy, August 26-31, 1985.

[10] H. H. Towner, R. J. Goldston, D. C. McCune, S. Tamor, Bull. Am. Phys. Soc. 26 (1981) 857.

[11] S. Tamor, J. Comput. Phys. 40 (1981) 104-119.

[12] K. T. Tsang, E. A. Frieman, Phys. Fluids 19 (1976) 747.

[13] A. H. Boozer, Phys. Fluids 23 (1980) 2283.

[14] K. C. Shaing, J. D. Callen, Phys. Fluids 25 (1982) 1012.

[15] T. E. Stringer, Nucl. Fusion 12 (1972) 689.

[16] J. W. Connor, R. J. Hastie, Nucl. Fusion 13 (1973) 24.

[17] K. C. Shaing, J. D. Callen, Nucl. Fusion 22 (1982) 1061.

[18] S. Scott, J. F. Lyon, J. K. Munro, D. J. Sigmar, et al., Nucl. Fusion 25 (1985) 359.

FIGURE CAPTIONS

FIG. 1. Experimental arrangement, showing a quadrant of the TFTR vacuum vessel, the pre(post)compression plasmas and the spectrometer sightline. The angle α of the intersection between the spectrometer right line and the major radius R of the plasma center is given by Eq. (2): $R \sin \alpha = D$, where D is the distance of the sight line from a parallel diameter of the torus.

FIG. 2. Time history of the plasma major radius R(t) during the compression as deduced from the laser scattering data.

FIG. 3. Time history of the observed wavelength shift $\Delta\lambda(t)$ of the Ti XXI Kα line at $\lambda = 2.6097$ Å. Subfigure (a) presents the data from a single discharge, and subfigures (b), (c) present accumulated data from eight discharges with nearly identical parameters. Accumulation of data from different discharges provides a reduction of satistical errors and averaging of the line displacements due to sawtooth events which are observed from the data of single discharges [subfigure (a)]. Interferences of the data from mechanical oscillations of the TFTR vacuum vessel after the compression at $t > 2.530$ sec are smoothed in subfigure (c) by choosing 80 msec time bins. The variation of the bulk plasma toroidal rotation during the compression stroke is evaluated from the data points labelled 1-5.

FIG. 4. Observed central toroidal rotation velocity $v_\phi(0)$ of the precompression plasma at the end of neutral deuterium beam injection vs the ratio of the beam power P_b and the line-averaged density $\bar{n}_e$.

FIG. 5. Time history of the wavelength shift $\Delta\lambda(t)$ as observed during the compression for all experimental conditions investigated. The experimental data are normalized to the value of $\Delta\lambda(0)$ obtained immediately before the compression, after termination of the neutral injection. Also shown are the values of $R(0)/R(t)$ and $[R(0)/R(t)]^2$ [curves (c) and (a), respectively] which are obtained from the curve fit to the laser scattering data shown in Fig. 2. The staircase, curve (b), is obtained by time averaging curve (a) over 10 msec intervals which corresponds to the time resolution of the Ti XXI Kα-measurements.

FIG. 6. (a) Measured and simulated central toroidal rotation speed during neutral injection and compression. The solid portion of the simulated velocity line represents the interval during which the momentum diffusivity was held fixed. The incident (r_i) and absorbed (r_a) beam torque are also shown.

(b) Time history of the global momentum confinement time τ_ϕ derived from the velocity simulation.

(c) Time history of the slowing-down time τ_s for the energetic beam ions. τ_s is the characteristic time for loss of the parallel velocity.

#86X0930

EXPERIMENTAL ARRANGEMENT

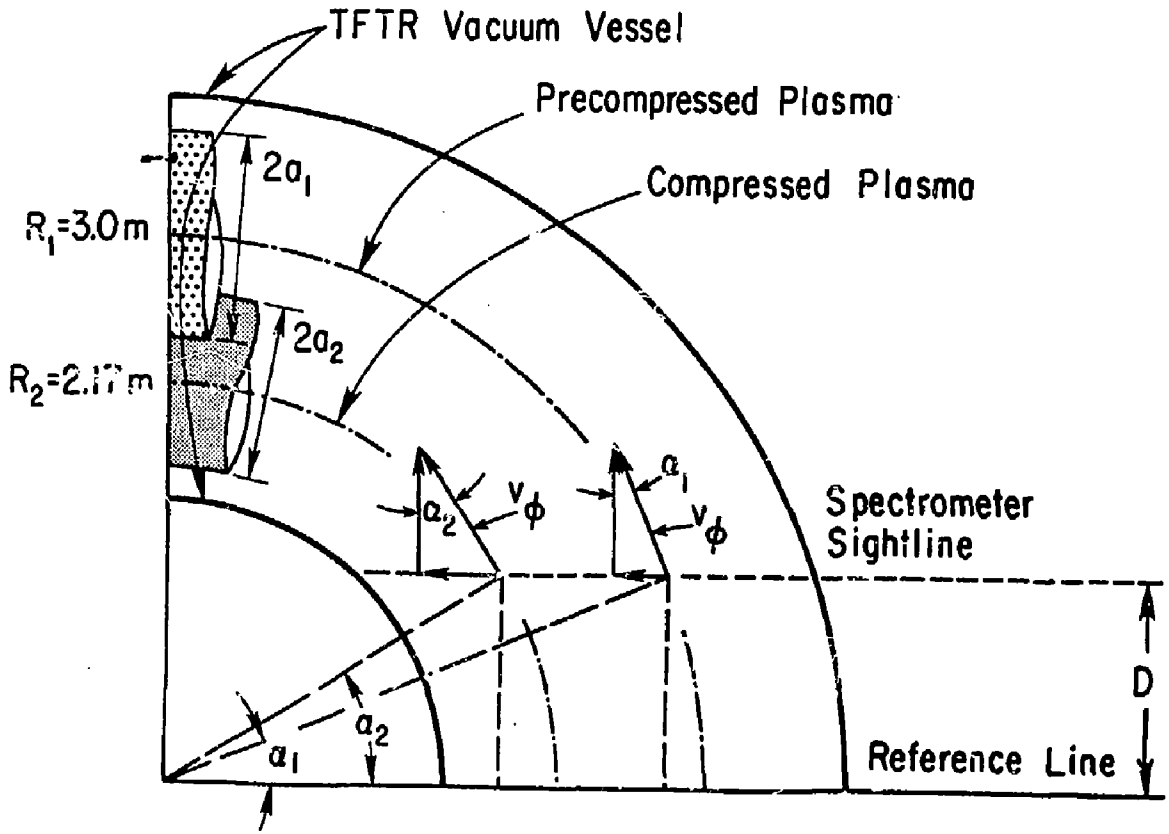

Fig. 1.

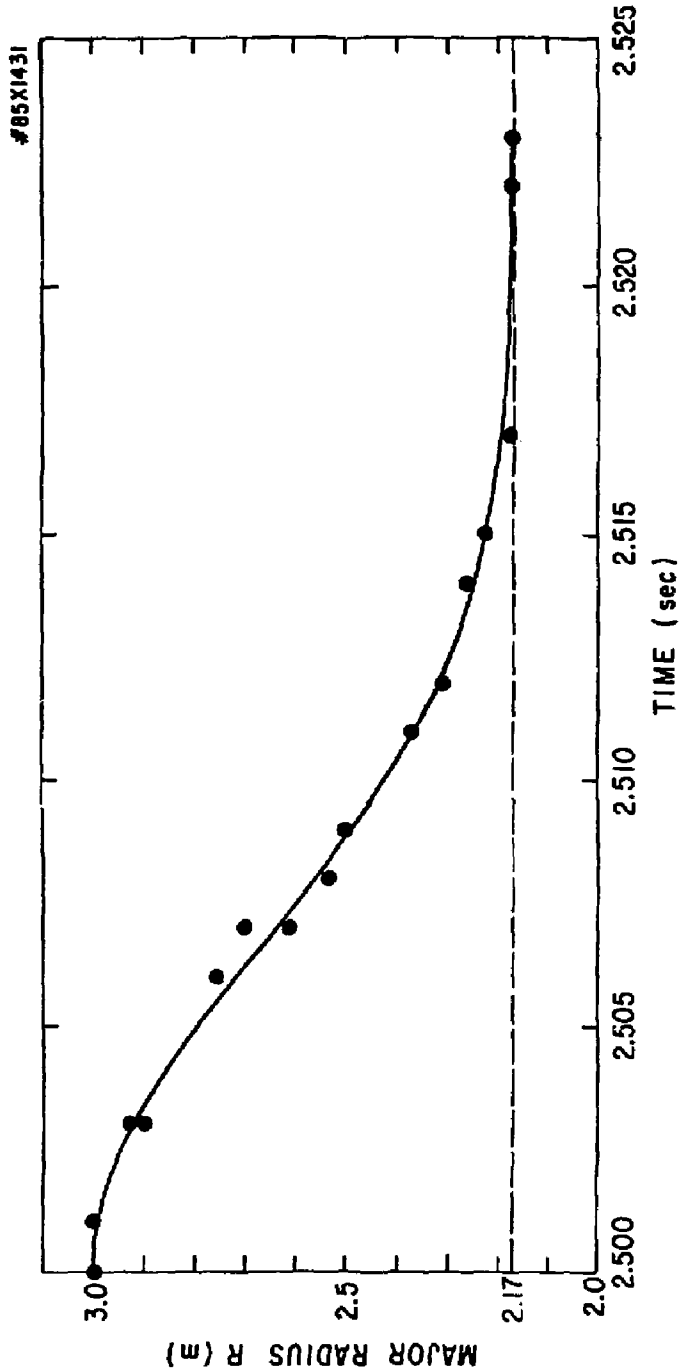
#85X1431
MAJOR RADIUS R (m)
3.0
2.5
2.17
2.0
2.500
2.505
2.510
2.515
2.520
2.525
TIME (sec)

Fig. 2.

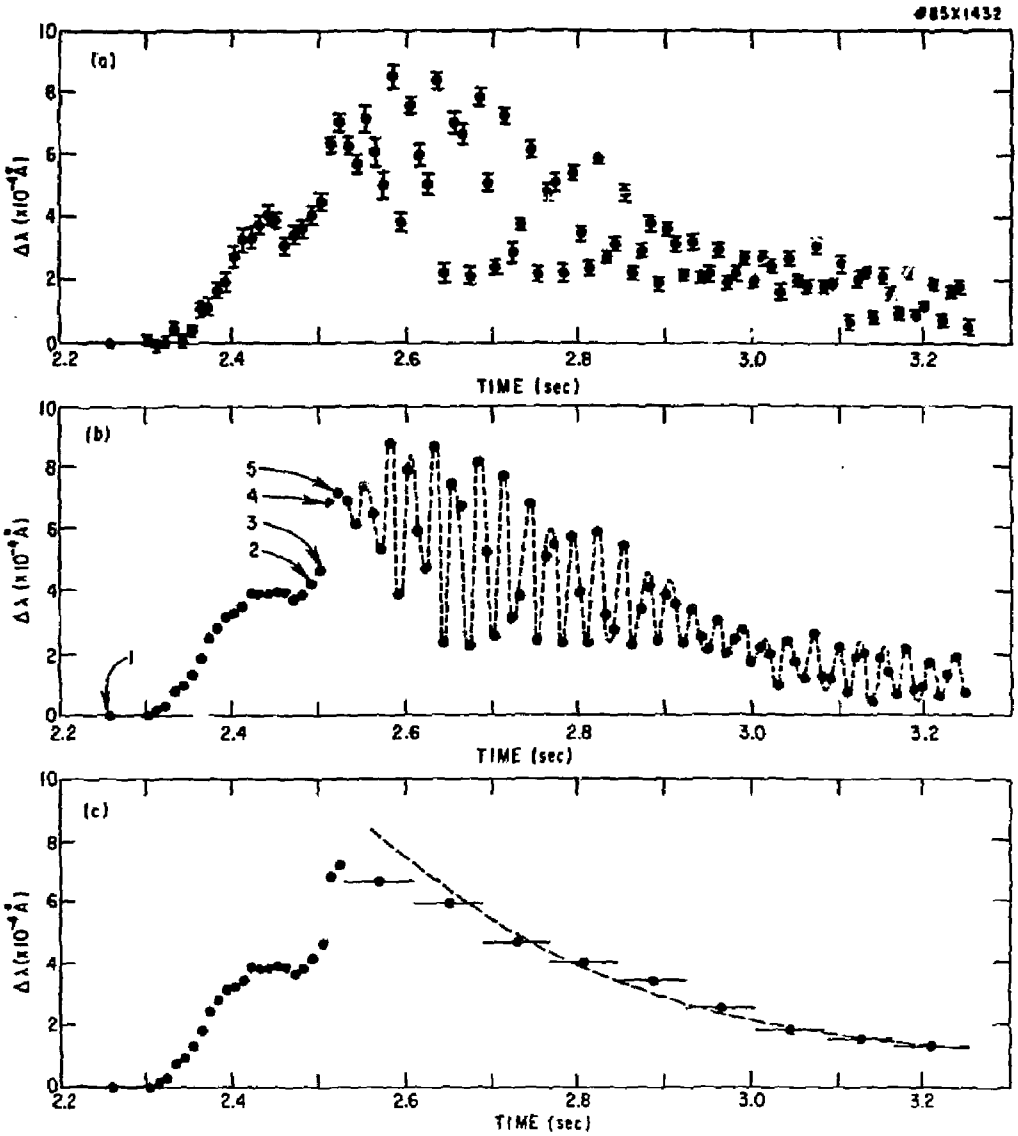

Fig. 3.

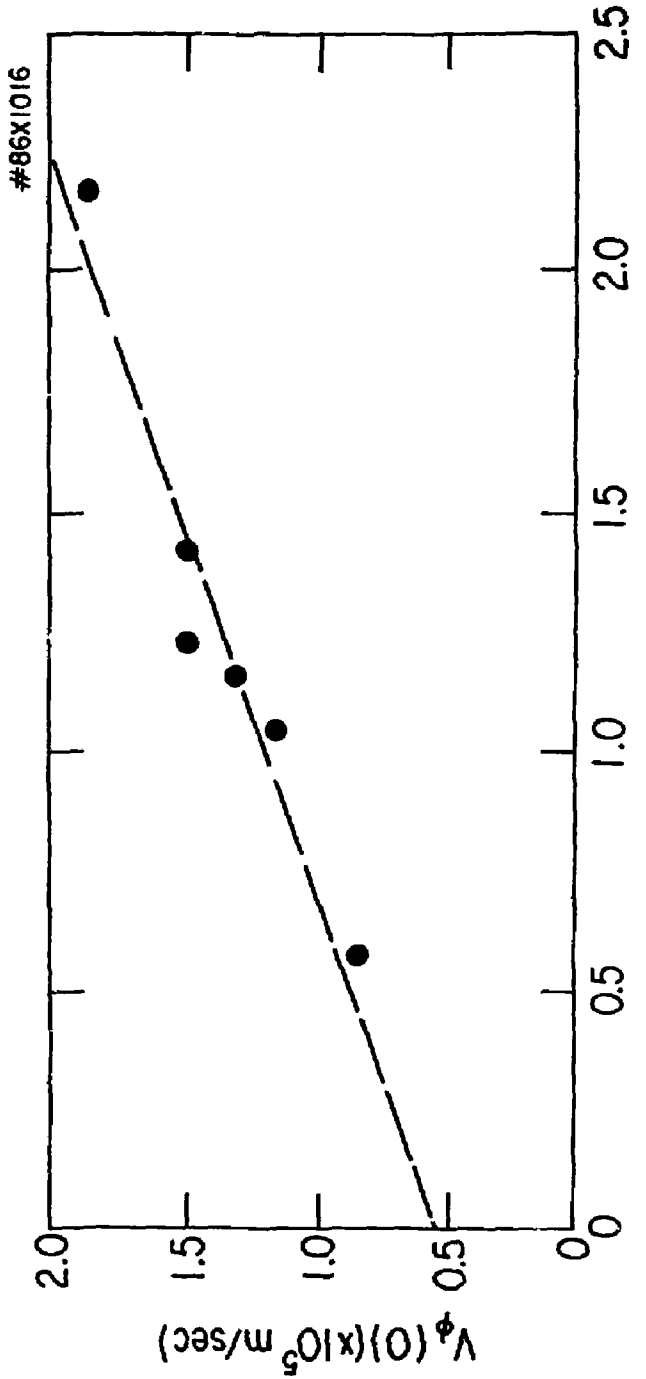
#86X1016
$V_\phi(0)(\times 10^5$ m/sec)
$P_b/\bar{n}_e$ ($\times 10^{-13}$ W·m^3)
0
0.5
1.0
1.5
2.0
2.5

Fig. 4.

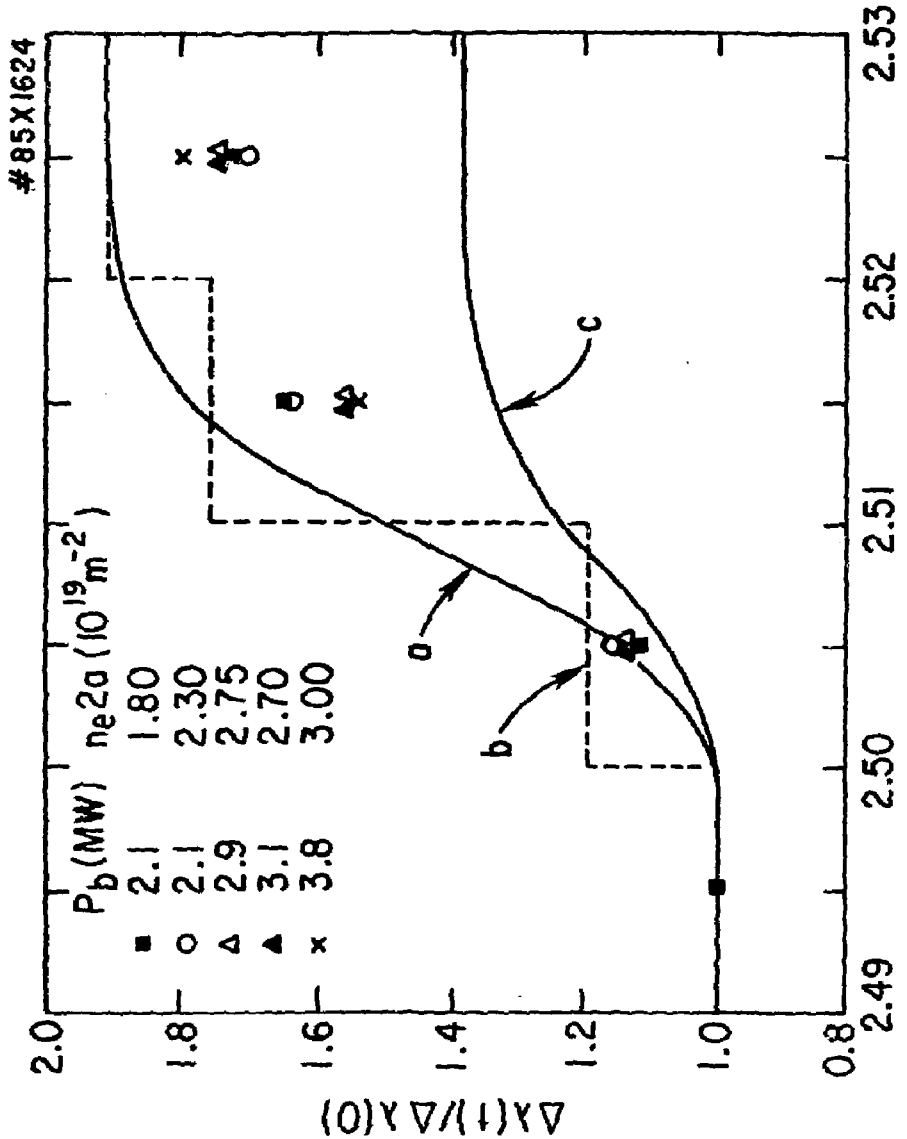
#85X1624
P_b(MW) $n_e 2a$ (10^{19} m^{-2})
■ 2.1 1.80
○ 2.1 2.30
△ 2.9 2.75
▲ 3.1 2.70
× 3.8 3.00
a
b
c
2.0
1.8
1.6
1.4
1.2
1.0
0.8
2.49
2.50
2.51
2.52
2.53
TIME (sec)
ΔX(1)/ΔX(0)

Fig. 5.

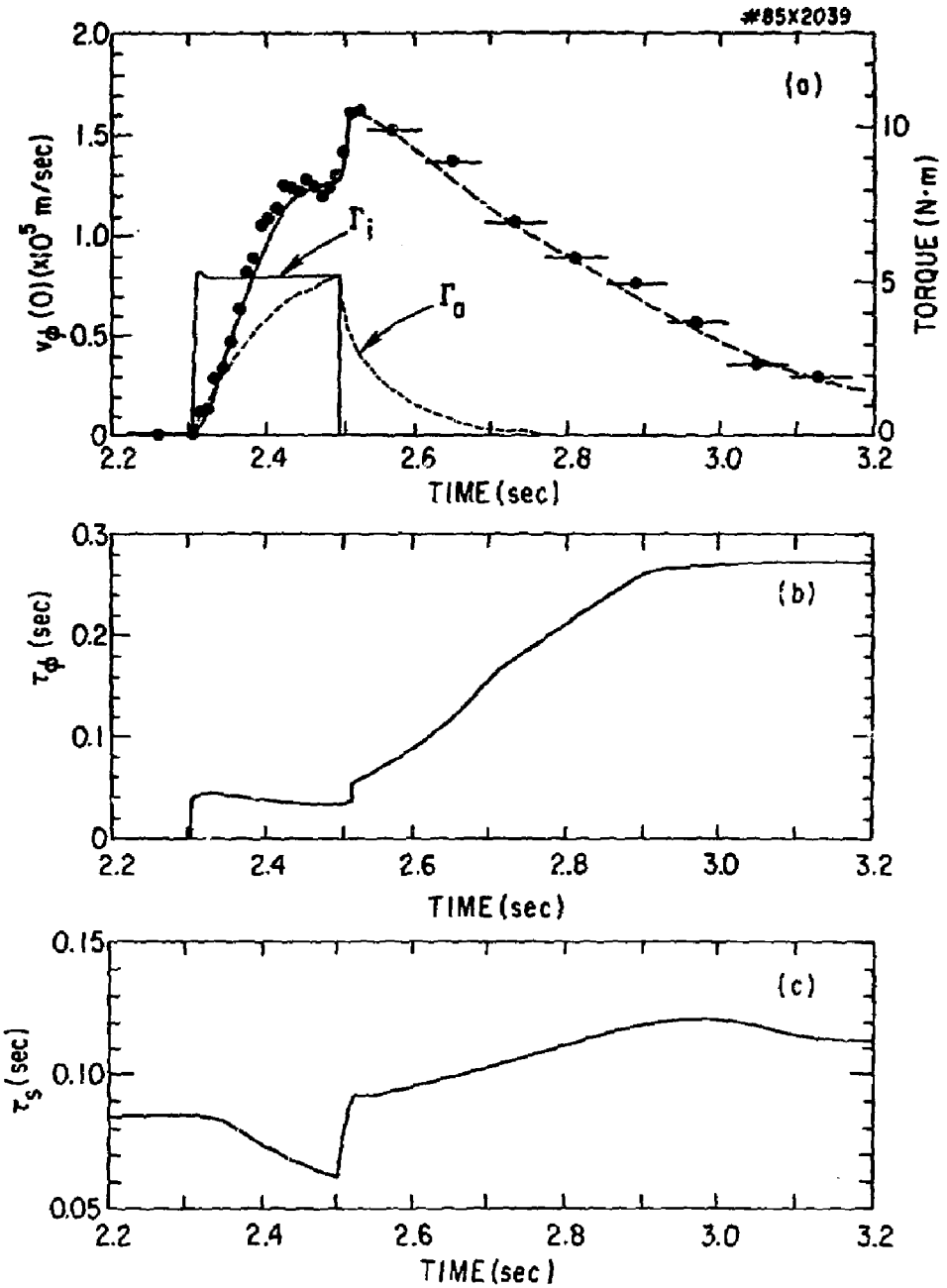
#85X2039
(a)
$v_\phi(0)$ (x10^5 m/sec)
TORQUE (N·m)
Γ_i
Γ_0
TIME (sec)
(b)
τ_ϕ (sec)
TIME (sec)
(c)
τ_s (sec)
TIME (sec)

Fig. 6.

EXTERNAL DISTRIBUTION IN ADDITION TO UC-20

Plasma Res Lab, Austra Nat'l Univ, AUSTRALIA
Dr. Frank J. Paoloni, Univ of Wollongong, AUSTRALIA
Prof. I.R. Jones, Flinders Univ., AUSTRALIA
Prof. M.H. Brennan, Univ Sydney, AUSTRALIA
Prof. F. Cap, Inst Theo Phys, AUSTRIA
M. Goossens, Astronomisch Instituut, BELGIUM
Prof. R. Boucique, Laboratorium voor Natuurkunde, BELGIUM
Dr. D. Palumbo, Dg XII Fusion Prog, BELGIUM
Ecole Royale Militaire, Lab de Phys Plasmas, BELGIUM
Dr. P.H. Sakanaka, Univ Estadual, BRAZIL
Lib. & Doc. Div., Instituto de Pesquisas Espaciais, BRAZIL
Dr. C.R. James, Univ of Alberta, CANADA
Prof. J. Teichmann, Univ of Montreal, CANADA
Dr. H.M. Skarsgard, Univ of Saskatchewan, CANADA
Prof. S.R. Sreenivasan, University of Calgary, CANADA
Prof. Tudor W. Johnston, INRS-Energie, CANADA
Dr. Hannes Barnard, Univ British Columbia, CANADA
Dr. M.P. Bachynski, MPB Technologies, Inc., CANADA
Chalk River, Nucl Lab, CANADA
Zhengwu Li, SW Inst Physics, CHINA
Library, Tsing Hua University, CHINA
Librarian, Institute of Physics, CHINA
Inst Plasma Phys, Academia Sinica, CHINA
Dr. Peter Lukac, Komenskeho Univ, CZECHOSLOVAKIA
The Librarian, Culham Laboratory, ENGLAND
Prof. Schatzman, Observatoire de Nice, FRANCE
J. Radat, CEN-BP6, FRANCE
JET Reading Room, JET Joint Undertaking, ENGLAND
AM Dupas Library, AM Dupas Library, FRANCE
Dr. Tom Mual, Academy Bibliographic, HONG KONG
Preprint Library, Cent Res Inst Phys, HUNGARY
Dr. R.K. Chhajlani, Vikram Univ, INDIA
Dr. B. Dasgupta, Saha Inst, INDIA
Dr. P. Kaw, Physical Research Lab, INDIA
Dr. Phillip Rosenau, Israel Inst Tech, ISRAEL
Prof. S. Cuperman, Tel Aviv University, ISRAEL
Prof. G. Rostagni, Univ Di Padova, ITALY
Librarian, Int'l Ctr Theo Phys, ITALY
Miss Clelia De Palo, Assoc EURATOM-ENEA, ITALY
Biblioteca, del CNR EURATOM, ITALY
Dr. H. Yamato, Toshiba Res & Dev, JAPAN
Direc, Dept. Lg. Tokamak Dev, JAERI, JAPAN
Prof. Nobuyuki Inoue, University of Tokyo, JAPAN
Research Info Center, Nagoya University, JAPAN
Prof. Kyoji Nishikawa, Univ of Hiroshima, JAPAN
Prof. Sigaru Mori, JAERI, JAPAN
Prof. S. Tanaka, Kyoto University, JAPAN
Library, Kyoto University, JAPAN
Prof. Ichiro Kawakami, Nihon Univ, JAPAN
Prof. Satoshi Itoh, Kyushu University, JAPAN
Dr. D.I. Choi, Adv. Inst Sci & Tech, KOREA
Tech Info Division, KAERI, KOREA
Bibliotheek, Fom-Inst Voor Plasma, NETHERLANDS
Prof. B.S. Liley, University of Waikato, NEW ZEALAND
Prof. J.A.C. Cabral, Inst Superior Tecn, PORTUGAL
Dr. Octavian Petrus, ALI CUZA University, ROMANIA
Prof. M.A. Hellberg, University of Natal, SO AFRICA
Dr. Johan de Villiers, Plasma Physics, Nucor, SO AFRICA
Fusion Div. Library, JEN, SPAIN
Prof. Hans Wilhelmson, Chalmers Univ Tech, SWEDEN
Dr. Lennart Stenflo, University of UMEA, SWEDEN
Library, Royal Inst Tech, SWEDEN
Centre de Recherchesen, Ecole Polytech Fed, SWITZERLAND
Dr. V.T. Tolok, Kharkov Phys Tech Ins, USSR
Dr. O.D. Ryutov, Siberian Acad Sci, USSR
Dr. G.A. Eliseev, Kurchatov Institute, USSR
Dr. V.A. Glukhikh, Inst Electro-Physical, USSR
Institute Gen. Physics, USSR
Prof. T.J.M. Boyd, Univ College N Wales, WALES
Dr. K. Schindler, Ruhr Universitat, W. GERMANY
ASDEX Reading Rm, IPP/Max-Planck-Institut fur Plasmaphysik, F.R.G.
Nuclear Res Estab, Julich Ltd, W. GERMANY
Librarian, Max-Planck Institut, W. GERMANY
Bibliothek, Inst Plasmaforschung, W. GERMANY
Prof. R.K. Janev, Inst Phys, YUGOSLAVIA